JOURNAL OF MATERIALS SCIENCE 29 (1994) 1940–1948

Sintering and microstructural development of ceria–gadolinia dispersed powders

P. DURÁN, C. MOURE, J. R. JURADO
Instituto de Cerámica y Vidrio (CSIC), Electroceramics Department, 28500 Arganda del Rey, Madrid, Spain

Well-dispersed ceria–gadolinia oxide powders were obtained from thoroughly isopropanol-washed coprecipitated oxalates, followed by calcination at 800 °C. The characteristics of the calcined powders and the microstructure of the green compacts were found to be of great importance in the sintering behaviour. Those green bodies in which some agglomerate survived after compaction reached a lower final density, while those having soft agglomerates were almost fully densified at a sintering temperature as low as 1400 °C. The densification process was studied by isothermal and constant heating rate dilatometry, and microstructural development at each stage in the processing was followed by SEM. By controlling the processing variables it was possible to obtain low-temperature near fully dense (better than 99%) and tough CeO_2–Gd_2O_3 bodies with homogeneous microstructure.

1. Introduction

Cerium dioxide when doped with divalent cations (Ca^{2+}, Mg^{2+}) or trivalent ones (La^{3+}, Y^{3+}, Gd^{3+}, etc.) forms a solid solution with the fluorite structure having an oxygen vacancies concentration depending on the amount of the dopant cation. Such a solid solution, similar to those of the calcia- and yttria-stabilized zirconias, shows an entirely ionic conductivity in air below 1000 °C, or mixed conductivity (MC) in a low oxygen atmosphere, as reported by Kudo and Obayashi [1, 2] and Dirstine *et al.* [3]. This being so, ceria-doped ceramics could be considered as good electrolytes or electrodes for high-temperature fuel cells (SOFC) and as oxygen sensors [4]. However, the electrical performances of these ceramic materials are strongly influenced by several factors, e.g. (a) dopant size and concentration which, above a critical amount, leads to the formation of ordered structures with the subsequent decrease of the electrical conductivity, (b) purity, composition homogeneity, density, and microstructural uniformity of the ceria-doped ceramics leading to a clearer a.c. behaviour related to both the grains and the grain-boundary impedances, and (c) the grain boundaries which act as depressors of d.c. conductivity as a consequence of a blocking effect of the charge carriers.

To overcome some of the above difficulties, Riess *et al.* [5] tried to correlate density and ionic conductivity of sintered $Ce_{1-x}Gd_xO_{2-x/2}\square_{x/2}$ ($\square$ is an oxygen vacancy) ceramics prepared by both the conventional mixed oxides and the non-conventional coprecipitation methods. The main conclusion found was a different gadolinium concentration in the grain bulk and grain boundaries. Therefore, the necessity of a good homogeneity for achieving a high ionic conductivity was evinced. In the same way, Dragoo and Domingues [6] studied the a.c. impedance properties of the chemically prepared oxides comparatively with those of the conventional mixed oxides in the case of hot-pressed $Ce_{1-x}Y_xO_{2-x/2}\square_{x/2}$ ceramics. Once more a better yttrium distribution was found in the case of the chemically prepared Y-CeO_2 ceramics, and well-resolved lattice and grain-boundary impedances were achieved. Microstructure, residual porosity location, and grain size of the sintered bodies were considered to be important factors in its electrical behaviour. Gerhardt and Nowick [7] and Gerhardt *et al.* [8] reported the strong influence of the grain boundaries in reducing the ionic conductivity of $Ce_{1-x}Ln_xO_{2-x/2}\square_{x/2}$ (Ln = Y, Gd, La) ceramics. The effects of dopant size, dopant concentration, porosity and sintering time of the ceria-doped ceramics on their electrical performances were also studied. It seemed to be that an amorphous silica-rich phase surrounding grain boundaries was responsible for the "grain-boundary effect". Some discrepancies with this conclusion have been reported by Beekmans and Heyne [9] and Bonanos *et al.* [10] in calcia-stabilized cubic zirconia and tetragonal polycrystalline zirconia, respectively, in which an inhomogeneous compositional distribution was the main factor causing the particular impedance behaviour of these electrolytes.

Recently, Riess [11] considered the possibility of using these types of MC ceramics instead of electrolytes in fuel cells, and Eguchi *et al.* [12] reported the electrical properties of several ceria-doped oxides and their application to solid oxide fuel cells (SOFC), concluding that samarium- and gadolinium-doped ceria ceramics were the best candidates.

Although the electrical performance of ceria-based oxides are coming to be considered as reasonably good candidates for SOFC systems, some parameters, such as the mechanical properties, chemical stability, thermal expansion, and thermal shock resistance,

0022–2461

should be strongly enhanced, and this is only possible by controlling the processing of these ceramics or designing new ceramic compositions.

In view of the extreme importance of both the powder preparation method and the sintering as key steps in determining both the microstructure and the performance of these ceramics, the goal of the present work was to evaluate the characteristics of the CeO_2–Gd_2O_3 dispersed powders in developing homogeneous microstructures through a controlled sintering process.

2. Experimental procedure

$Ce(NO_3)_3 \cdot 6H_2O$ and $Gd(NO_3)_3 \cdot 6H_2O$ were used as the starting materials. The supplier's analysis indicated the presence of several impurities in the $Ce(NO_3)_3 \cdot 6H_2O$, mainly silicon, calcium, iron, sodium and potassium at several tens p.p.m. The impurity level of $Gd(NO_3)_3 \cdot 6H_2O$ was not reported by the suppliers, though that was at least 99.9% pure. Ce–Gd nitrates in the appropriate amounts were dissolved in distilled water to give a stock solution which was diluted again with distilled water up to a 0.3 mol l^{-1} solution was attained.

The flow sheet for preparing the CeO_2–Gd_2O_3 powders can be seen in Fig. 1. The stock solution containing the required Ce–Gd composition Ce–4Gd (4 mol % Gd_2O_3) or Ce–8Gd (8 mol % Gd_2O_3) was added by dropping and blending to an aqueous oxalic acid solution containing 35 g l^{-1}. During the coprecipitation, a rigorous control of the pH (between 6.5 and 7) was maintained by the dropwise addition of diluted ammonia. When the coprecipitation process was completed, a small amount of diluted NH_4OH was added to precipitate any remaining cerium or gadolinium which could remain in the solution. After filtering, the precipitate was first washed with water, and then several times with isopropyl alcohol. The precipitate was slowly dried in air at 70–80 °C. Samples of the precipitates were studied using SEM, X-ray diffraction (XRD), and differential thermal analysis/thermogravimetric analysis (DTA/TGA). After calcining at 800 °C for 1 h, the powders were ball-milled for 1 h in isopropyl alcohol, dried, and examined by XRD, SEM and BET (nitrogen adsorption). The calcined powders were formed into a billet without binder, isostatically pressed at 200 MPa, and then air sintered in the temperature range 1200–1600 °C for 4 h. Disc-shaped specimens were cut from the billet for examination by XRD and SEM. The determination of the lattice constant was carried out by using a vertical computer-automated X-ray diffractometer with computer analysis of the rate. CuK_α radiation with a nickel filter was utilized. Only those peaks with angle $2\theta > 70°$ were scanned for these measurements. Bulk densities were measured by the Archimedes method using water as the liquid medium. The study of the sinterability of the Ce–4Gd and Ce–8Gd calcined powders was performed on the isopressed compacts by using a dilatometer. The heating and cooling rates were 5 °C min^{-1} and the sintering temperature was 1550 °C. Fracture surfaces from several samples were

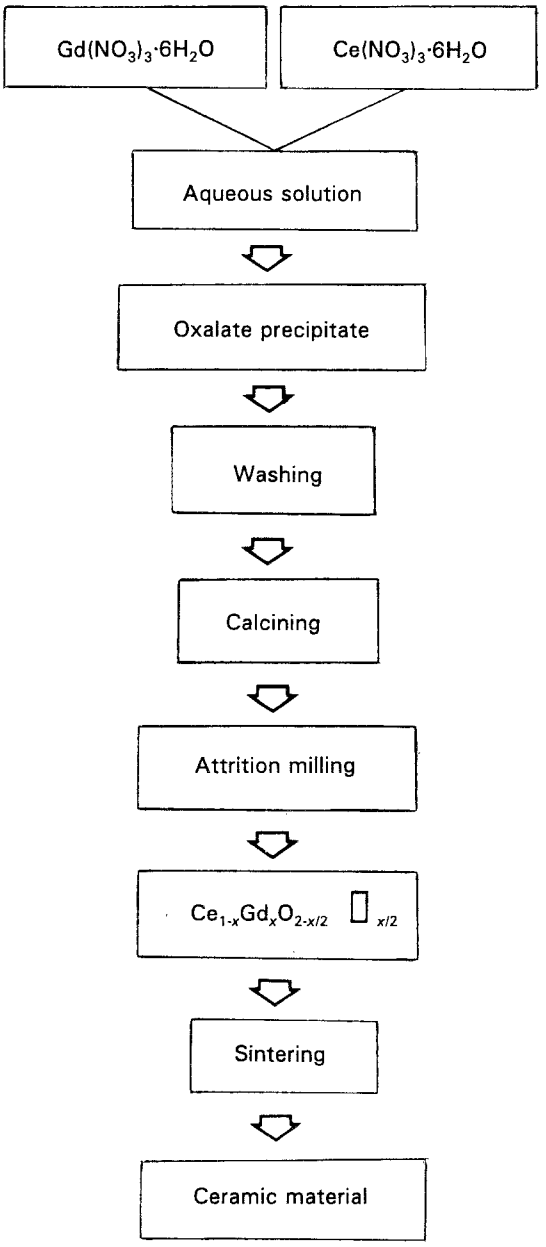

Figure 1 Flow sheet for the preparation of Ce–Gd oxalate powders.

examined by SEM, which also enabled the grain-size determinations on thermally etched polished surface samples. The homogeneity of the samples was determined by electron microprobe analysis. An inductively coupled plasma spectrometry (ICP–AES) technique was used to measure the impurities content of the sintered samples.

The mechanical measurements were carried out by the microindentation technique, and a load of 5 kg was used to measure the fracture toughness, K_{IC}, and Vickers hardness, H_v.

3. Results and discussion

3.1. Powder characteristics

As shown in Fig. 2b, the XRD pattern of the coprecipitated oxalate showed a crystalline phase whose diffraction lines could not be indexed either as cerium oxalate or as gadolinium oxalate, indicating that such a crystalline phase is not a mixture of the oxalates but a complex salt with an unknown formula. For comparison, in the same figure, XRD patterns of the

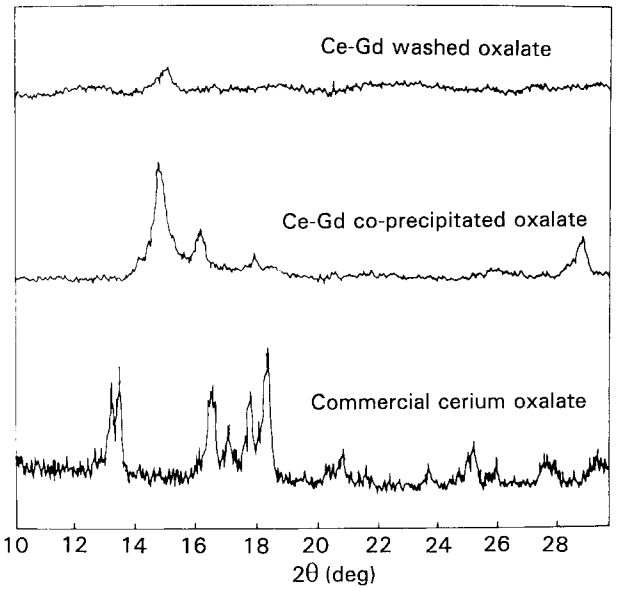

Figure 2 X-ray diffraction patterns of the Ce–Gd oxalates.

cerium oxalate (a) and that of the thoroughly washed coprecipitated oxalate (c) are also shown. It can be observed that the XRD peaks of the coprecipitated oxalate were greatly weakened by an intensive isopropanol washing leading to an almost amorphous one. Similar results were achieved by Yamamura *et al.* [13] in the case of PLZT oxalate prepared powders by washing with ethanol.

Fig. 3 shows the DTA/TGA curves registered on the amorphous oxalate and, as can be seen, the water of hydration was driven off at approximately 250 °C, and then the oxalate decomposed at ~ 340 °C; no other thermal effects were present at higher temperature. The final weight loss of the amorphous oxalate reached ~ 59%. If it is assumed that weight loss arises from both thermal decomposition of oxalate ions and vaporization of water of hydration, and taking into account that the theoretical weight loss of a double cerium and gadolinium oxalate without water of hydration is approximately 47%, then the water content of the amorphous oxalate was estimated to be ~ 4 mol per unit chemical formula. The calculated amount of water of hydration, 3.74 mol, slightly smaller than that corresponding to the coprecipitation reaction, seems to be due to the effect of the isopropanol washing.

The Ce–4Gd and Ce–8Gd oxalate particles obtained by the above process from a nitrate solution exhibited a rod-like structure having an irregular prismatic shape which was retained after calcining. Calcining the coprecipitated powders at 800 °C for 1 h leads to a powder with a particle morphology as shown in Fig. 4A and B. A relatively well-dispersed powder with microcracked and porous particles retaining the prismatic shape was obtained, and their dimensions varied from 0.5–2.5 μm length and 0.1 μm width. Calcination of the coprecipitates converted these to a

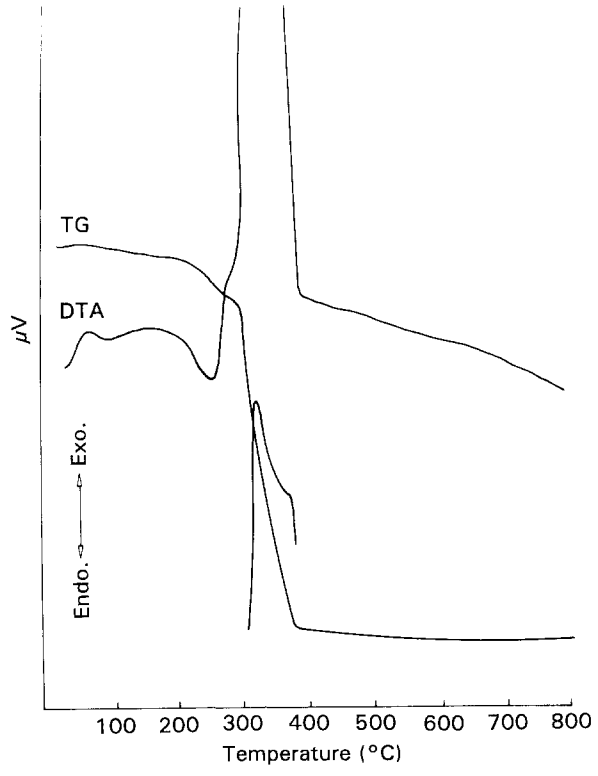

Figure 3 DTA/TGA curves for the Ce–Gd amorphous oxalate.

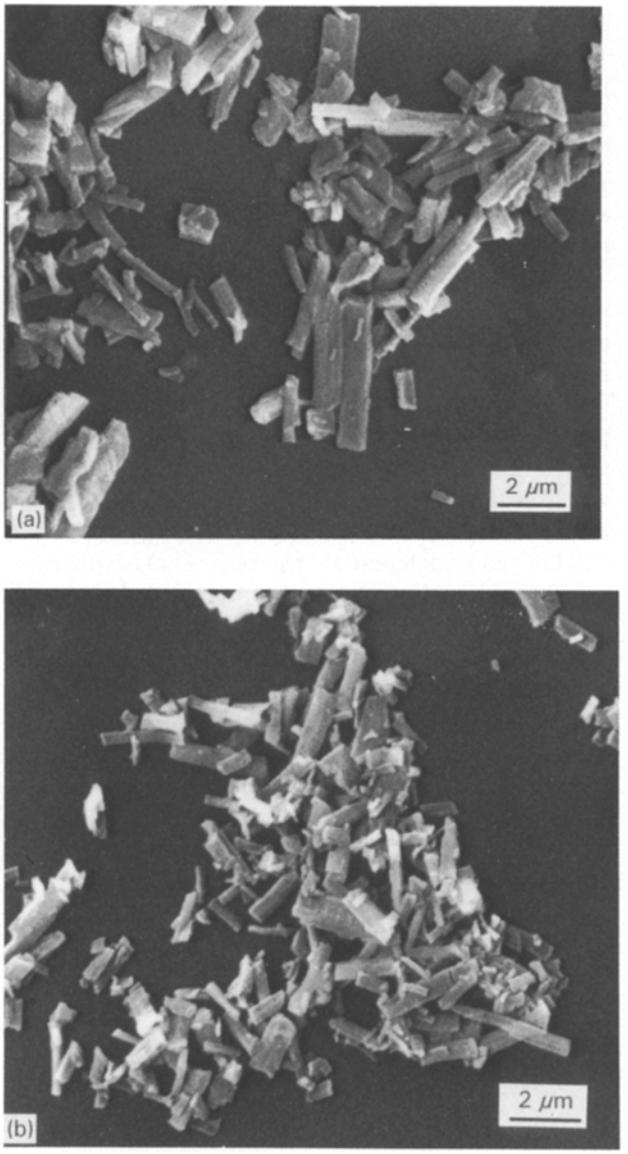

Figure 4 Scanning electron micrographs of the Ce–4Gd and Ce–8Gd calcined powders.

fluorite-structure material whose XRD patterns showed weak and very broad diffraction maxima. An estimation of the crystallite size was made from the broadened diffraction maxima of the calcined powders. The crystallite sizes measured were 30 and 41 nm for Ce–4Gd and Ce–8Gd, respectively. Fig. 5 shows the particle-size distribution curves for Ce–4Gd and Ce–8Gd powder samples after calcining at 800 °C for 1 h. The average particle sizes were approximately 3 and 1.5 μm, respectively. Differences in the particle size measured by SEM observations and that from the sedimentation technique arise as a consequence of the particle agglomeration state. It is believed that the average particle size measured using the sedimentation technique is rather an average of the agglomerate size.

The surface-area values as measured by the BET method were 55 and 64 $m^2 g^{-1}$ for the Ce–4Gd and Ce–8Gd calcined powders, respectively. For comparison, the values of surface area obtained from the expresion, $D = 6/\rho S$, taking into account both the crystallite size measured by X-ray diffraction and picnometric powder density, were 28 and 20 $m^2 g^{-1}$.

3.2. Isothermal sintering

The two calcined powders Ce–4Gd and Ce–8Gd isostatically pressed at 200 MPa, presented a similar green density (~ 40% theoretical density). However, the microstructure of the green compacts was more uniform in the case of the Ce–8Gd samples. As can be seen in Fig. 6A and B, scanning electron micrographs obtained on fractured green compacts show that hard prismatic agglomerates survived in the Ce–4Gd samples whilst they have been broken in the case of the Ce–8Gd samples, and a more uniform particle-size distribution can also be observed.

From the XRD studies the lattice parameters calculated on the Ce–4Gd and Ce–8Gd sintered samples were 0.5416 and 0.5418 ± 0.0005 nm, respectively, in good agreement with those measured by Bevan *et al.* [14] and McCullough *et al.* [15]. From these lattice parameters values and the composition of the two samples, the theoretical densities were calculated to be 7.22 and 7.24 g cm^{-3}, respectively.

Fig. 7 shows the isothermal sintering studies (4 h cycle) for the CeO_2–Gd_2O_3 powder compacts. In the case of the Ce–4Gd samples a densification as high as 91% theoretical density was achieved at 1300 °C, while only a 88% was obtained in the Ce–8Gd samples. Above that temperature the sintering process occurred very rapidly for the Ce–8Gd samples and these were 98% dense at 1400 °C and almost fully dense at 1500 °C. In this temperature range, the densification process for the Ce–4Gd was much slower, thus at 1400 °C the samples were 95% dense and only 98.5% dense at 1500 °C. Above that temperature, the density of the Ce–8Gd sintered samples decreased slightly and the density of the Ce–4Gd samples still increased. These results indicate that the sinterability of Ce–8Gd powder, as previously stated, was higher than that of Ce–4Gd powder.

The colour of the sintered samples varied from slightly yellow-beige (Ce–4Gd) to beige–cream for the

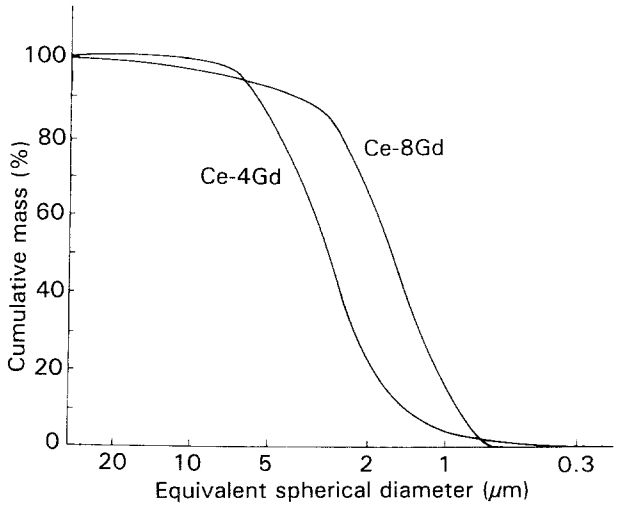

Figure 5 Particle-size distribution curves of the Ce–4Gd and Ce–8Gd calcined powders.

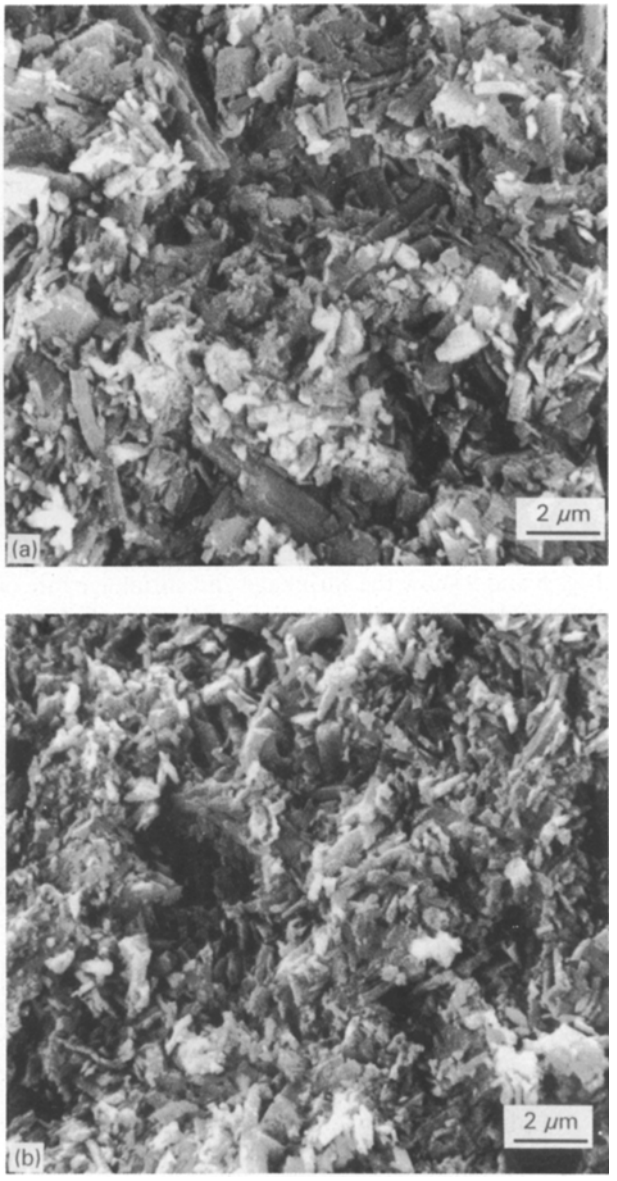

Figure 6 Scanning electron micrographs of fracture surface of Ce–4Gd and Ce–8Gd green compacts.

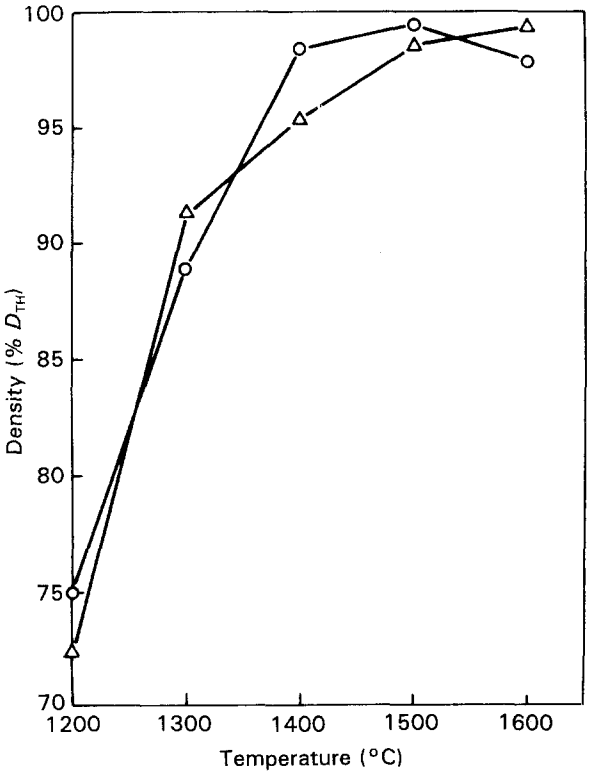

Figure 7 Isothermal sintered density of the (○) Ce–4Gd and (△) Ce–8Gd compacts as a function of temperature.

Ce–8Gd samples. The chemical composition of both samples after sintering, as determined by electron microprobe, was found to consist of 6.45 and 15.1 wt % Gd_2O_3, respectively. In both cases the Gd_2O_3 concentration slightly increased in the grain boundary.

The study of the impurity level present in the sintered samples showed a change with respect to the original composition, thus CaO (0.24 wt %), SiO_2 (660 p.p.m.), Na_2O (880 p.p.m.), K_2O (400 p.p.m.), and Al_2O_3 (200 p.p.m.). The increase in the impurities level probably resulted from the milling process.

3.3. Shrinkage behaviour

Figs 8 and 9 show the shrinkage and shrinkage rate of the powder compacts. Shrinkage of the Ce–4Gd compacts starts at about 400 °C with a first maximum rate at 700 °C in which a shrinkage of 12% was reached. A second and higher maximum rate was present at 1330 °C, and an end point was not achieved above 1500 °C for a shrinkage of approximately 23%. In the case of the Ce–8Gd compacts, the shrinkage starts at about the same temperature (360 °C) as that for Ce–4Gd compacts; however, the first maximum rate was located at 660 °C and a shrinkage of about 10%. The second maximum rate was present at about 1460 °C for a shrinkage of about 22%, and the end point was attained at about 1530 °C. The density of the compacts after this experiment was 6.93 and 7.13 $g\,cm^{-3}$ for the Ce–4Gd and Ce–8Gd samples, respectively.

Although a study of the evolution of the pore-size distribution in the sintered compacts was not made, from the microstructure evolution observed on both the polished and thermally etched and the fractured

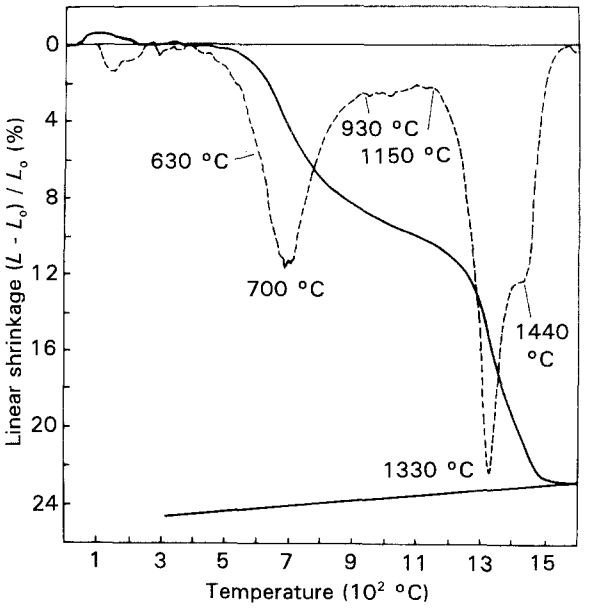

Figure 8 (——) Linear shrinkage and (– – –) shrinkage rate of Ce–4Gd green compacts.

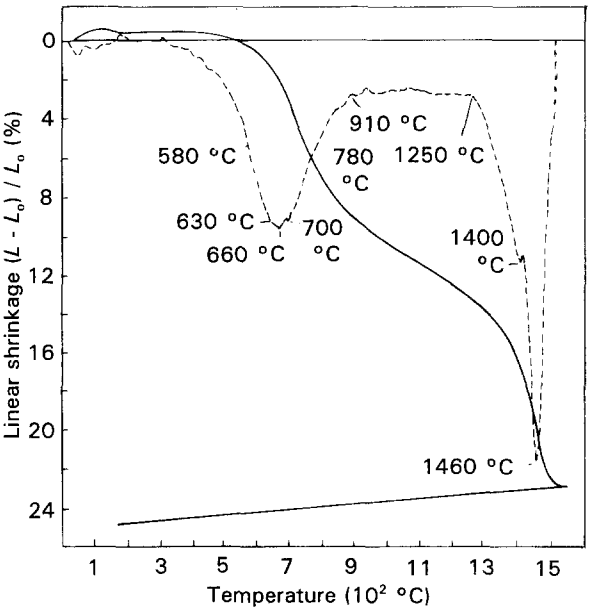

Figure 9 (——) Linear shrinkage and (– – –) shrinkage rate of Ce–8Gd green compacts.

surfaces of the green compacts heat-treated at different temperatures, it could be assumed that at low temperature (< 700 °C) in both kinds of sample the densification mechanism is similar. Thus below the two maxima at 700 and 660 °C, respectively, the intra-agglomerated porosity moves towards the interagglomerated pores and, in this way, the finer porosity is eliminated and a rise in the size of the pores between agglomerates takes place with a slight densification.

In the region of 700 and about 950 °C, the shrinkage rate significantly decreases. Such a decrease should be associated, according to the XRD results, with the solid solution $Ce_{1-x}Gd_xO_{2-x/2}\square_{x/2}$ reaction formation. Effectively in this temperature range, a transition from the almost amorphous phase to a polycrystalline one took place. This solid solution

reaction formation apparently does not modify the volume porosity. When such a phase reaction formation is complete (at 1150 and 1250 °C, respectively), the densification of the compacts progresses and the shrinkage rate increases again, attaining a maximum at 1330 and 1460 °C for Ce–4Gd and Ce–8Gd ceramic compacts, respectively. In both maxima the sintering rate of the respective cubic solid solutions is maximum. At those temperatures, the densities of the samples were ~90% and 97% dense, respectively, which are in good agreement with the isothermal sintering results.

3.4. Microstructural development

Fig. 10 shows the SEM fracture surfaces for samples Ce–4Gd and Ce–8Gd sintered at 1200–1600 °C. These micrographs, in accordance with the data in Fig. 7, illustrate the more rapid densification process which takes place as temperature is increased. The microstructural comparison seen in Fig. 10 shows a striking similarity between the two kinds of sintered samples. The less agglomerated Ce–8Gd powder produced a more uniform microstructure reaching a final density of better than 99.5% theoretical density. The small differences in microstructure were produced by packing geometry of the initial compacts, this being more favourable in the Ce–8Gd samples. In a general sense, the densification process took place through the formation of regions with higher density than others, and these denser areas could cause the appearance of different populations of pores, neck sizes and, in some cases, an exaggerated grain growth.

From the above sets of micrographs several important microstructural features could be emphasized. For example, transgranular fracture was already observed from the lower sintering temperatures and such a mode of fracture is unusual for ceramics with a grain size as small as 1–2 μm and, therefore, with a high grain-boundary density. On the other hand, neither

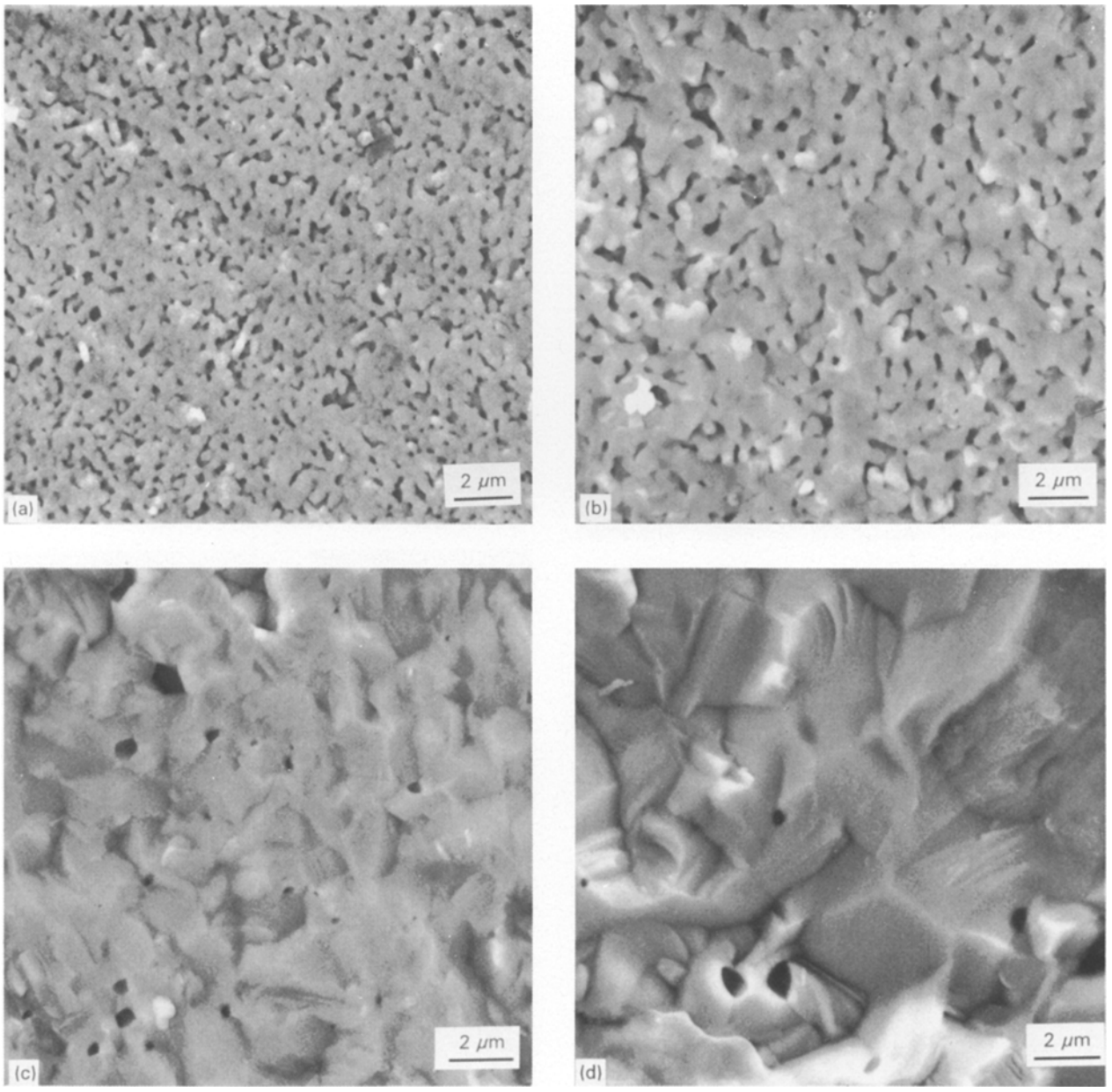

Figure 10 Scanning electron micrographs of fracture surface of (a–e) Ce–4Gd and (f–j) Ce–8Gd sintered compacts. (a, f) 1200 °C; (b, g) 1300 °C; (c, h) 1400 °C; (d, i) 1500 °C, (e, j) 1600 °C.

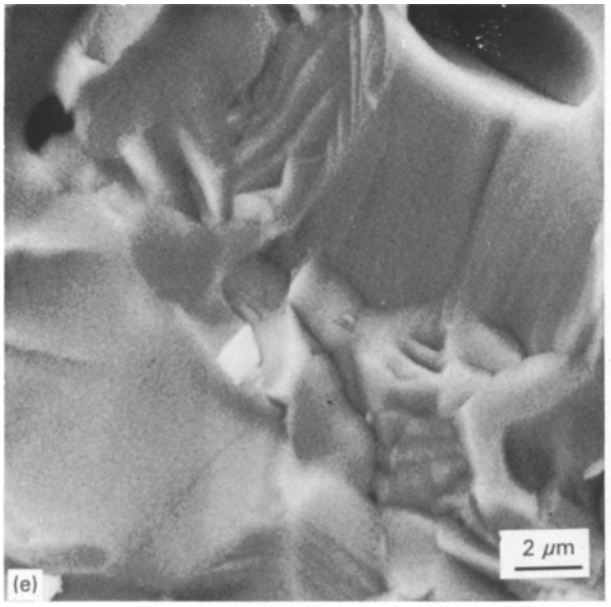

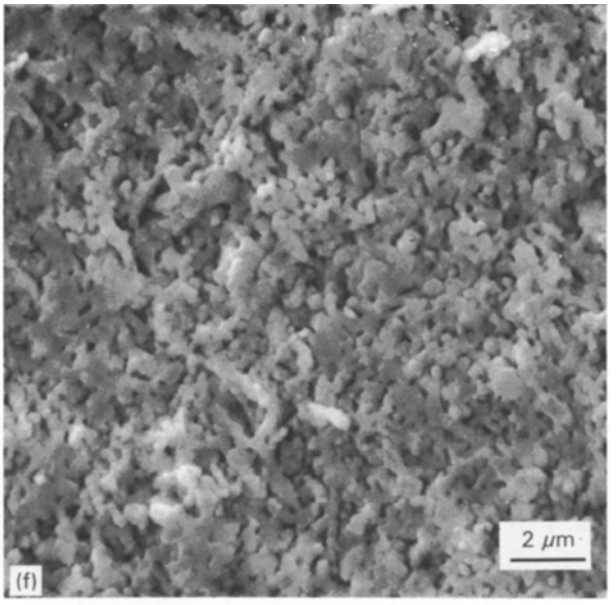

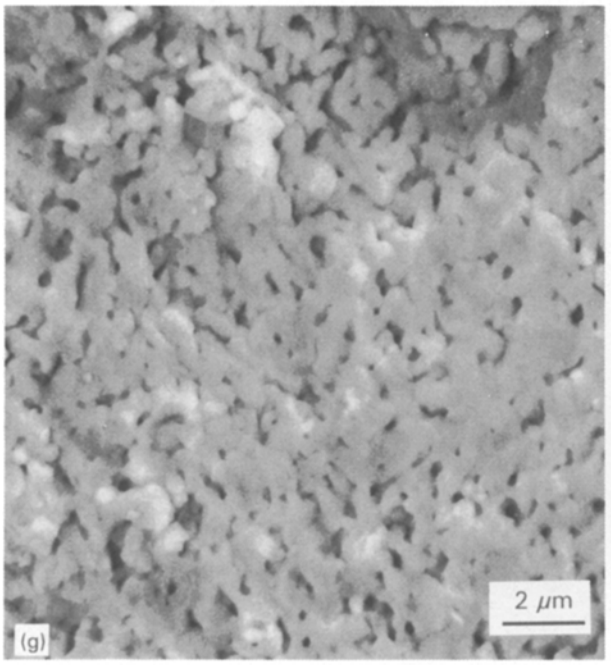

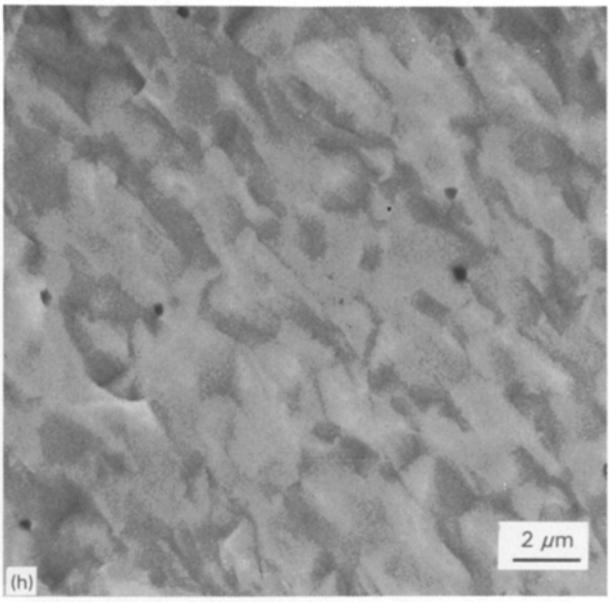

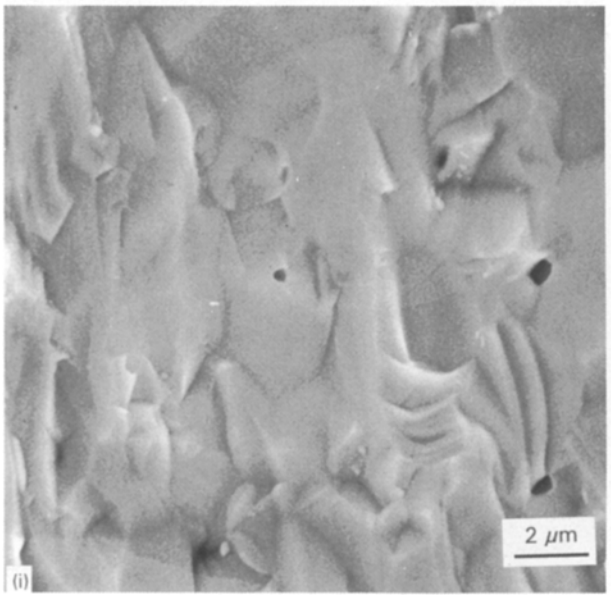

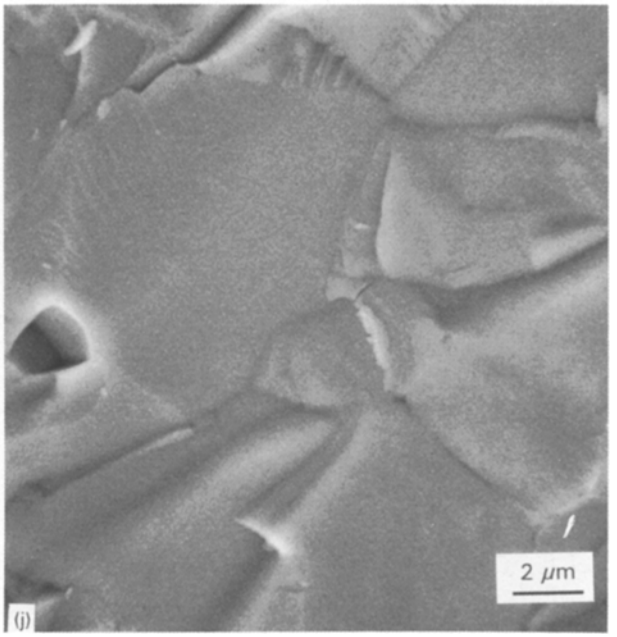

Figure 10 (Continued)

coarsening nor exaggerated grain growth was present in the sintered samples. No intragranular porosity was observed and all the pores were located at the grain boundaries or in the triple points.

Fig. 11 shows the microstructure of the sintered and thermally etched Ce–4Gd and Ce–8Gd samples in the temperature range 1400–1600 °C. A little grain growth occurred which indicates that the grain boundaries had been pinned by the pores. Furthermore, a more rapid grain growth took place in the Ce–4Gd sintered samples which, probably, was a consequence of both the wider particle-size distribution and the less uniform packing. The fact that porosity remained at the grain boundaries and no exaggerated grain growth was produced is a result of the better Ce–8Gd dispersed powders.

3.5. Fracture toughness

Preliminary results of toughness measurements on the sintered Gd–doped ceria ceramics are given in Table I together with their grain sizes, microhardness, and Young's modulus. The values were obtained on samples having the same density. Comparatively, the K_{IC} values measured for these ceria-doped ceramics are higher than those currently reported for yttria-stabilized cubic zirconia electrolytes [16, 17].

4. Conclusion

Submicronized relatively well-dispersed CeO_2–Gd_2O_3 powders were obtained by calcining at 800 °C the corresponding thoroughly isopropanol-washed coprecipitated Ce–Gd oxalates. The sinterability of gadol-

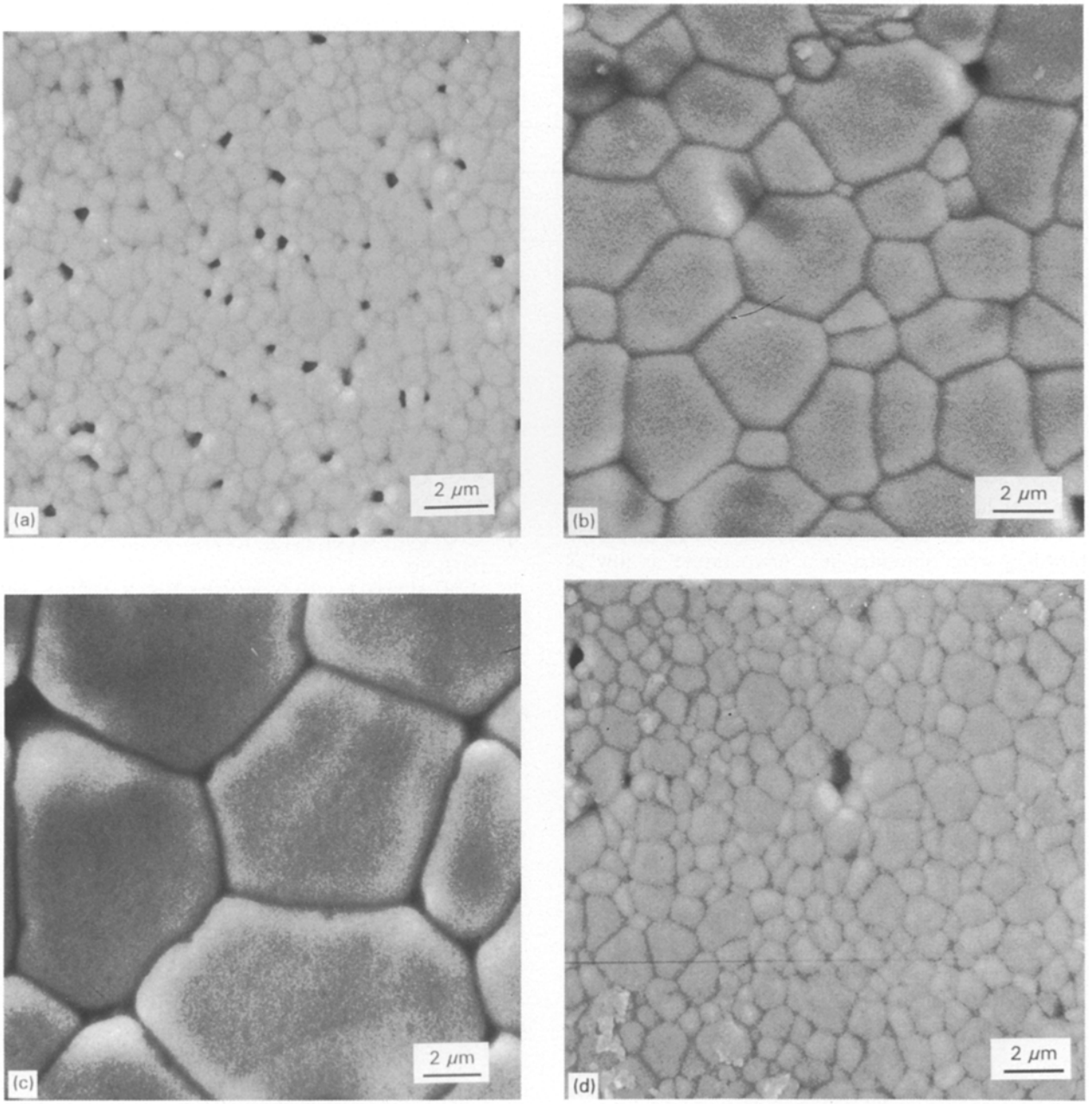

Figure 11 Scanning electron micrographs of polished and thermally etched (a–c) Ce–4Gd and (d–f) Ce–8Gd sintered samples. (a, d) 1400 °C, (b, e) 1500 °C, (c, f) 1600 °C.

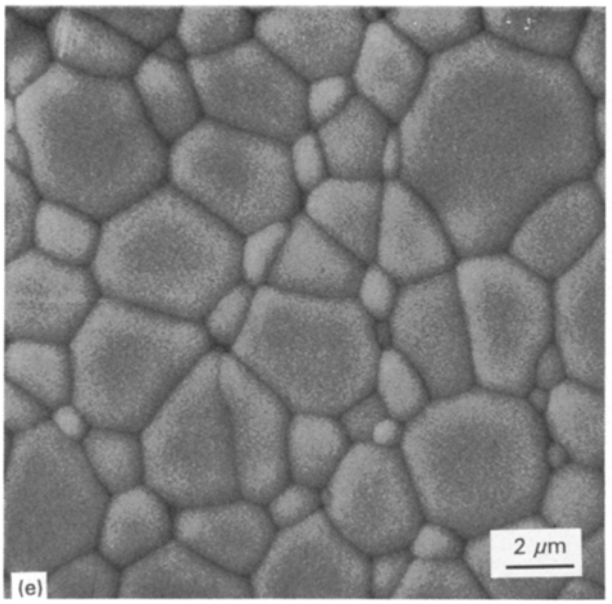

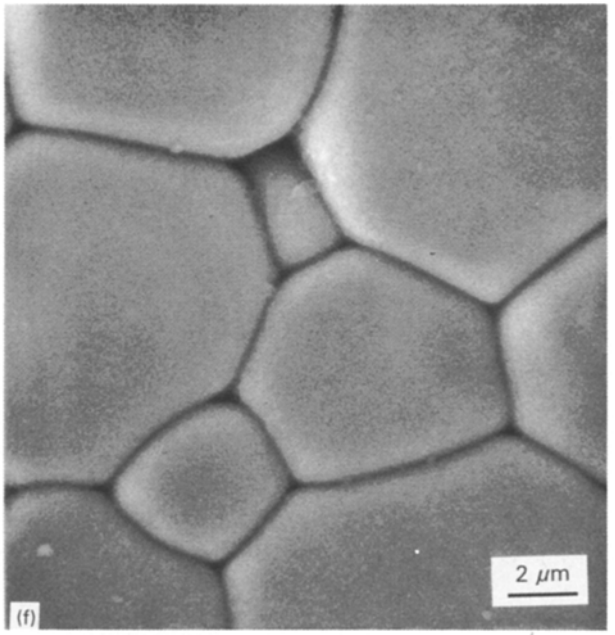

Figure 11 (Continued)

TABLE I

Sample	Density (%)	K_{IC} (MPa $m^{-1/2}$)	H_v	E (Nm^{-3})	Grain size (μm)
Ce–4Gd	98.6	3.2	7.8	175	4
Ce–8Gd	98.6	2.2	6.6	166	3

inium-doped ceria powders has been studied taking into account their powder characteristics and the microstructure of the green compacts. It has been found that after isopressing, some agglomerates survived which influences the final density of the sintered bodies. The densification process of CeO_2–Gd_2O_3 powder compacts has been studied by isothermal and constant heating-rate dilatometry, and dense bodies better than 98.5% theoretical density in well-dispersed powders were obtained at a temperature as low as 1400 °C. Microstructural development correlated well to the sintering process, and neither bimodal nor exaggerated grain growth occurred. Transgranular fracture was present in the sintered bodies and a fracture toughness, K_{IC}, as high as 2–3 MPa $m^{-1/2}$ could be measured.

Acknowledgement

The financial support from the Commission of the European Community, JOULE 0044C is gratefully acknowledged.

References

1. T. KUDO and H. OBAYASHI, *J. Electrochem. Soc.* **122** (1975) 142.
2. *Idem, ibid.* **123** (1976) 415.
3. R. T. DIRSTINE, R. N. BLUMENTHAL and T. F. KUECH, *ibid.* **126** (1979) 264.
4. B. C. H. STEELE, *Solid State Ionics* **12** (1984) 391.
5. J. RIESS, D. BRAUNSHTEIN and D. S. TANHAUSER, *J. Am. Ceram. Soc.* **64** (1981) 479.
6. A. L. DRAGOO and L. P. DOMINGUES, *ibid.* **65** (1982) 253.
7. R. GERHARDT and A. S. NOWICK, *ibid.* **69** (1986) 641.
8. R. GERHARDT, A. S. NOWICK, M. E. MOCHEL and J. DUMLER, *ibid.* **69** (1986) 647.
9. N. M. BEEKMANS and L. HEYNE, *Electrochim. Acta* **21** (1976) 303.
10. N. BONANOS, R. L. SLOTWINSKI, B. C. H. STEELE and E. P. BUTLER, *J. Mater. Sci. Lett.* **3** (1984) 245.
11. I. RIESS, *Solid State Ionics* **52** (1992) 127.
12. K. EGUCHI, T. SETOGUCHI, T. INOUE and H. ARAI, *ibid.* **52** (1992) 165.
13. H. YANANURA, M. TANADA, H. HANEDA, S. SHIRASAKI and Y. MORIYOSHI, *Ceram. Int.* **11** (1985) 23.
14. D. J. M. BEVANM, W. W. BARKER and T. C. PARKS, in "Proceedings of the 4th Conference on Rare-Earth Research", edited by L. Eyring (Gordon and Breach, New York, 1965) p. 441.
15. J. D. McCULLOUGH and J. D. BRITTON, *J. Am. Chem. Soc.* **74** (1952) 5225.
16. T. K. GUPTA, F. F. LANGE and J. H. BETCHOLD, *J. Mater. Sci.* **13** (1978) 1464.
17. F. F. LANGE, *ibid.* **17** (1982) 240.

Received 12 October
and accepted 1 November 1993